P H Y S I C A L   R E V I E W   L E T T E R S

Nonequilibrium Sedimentation of Colloids on the Particle Scale

C. Patrick Royall,[1,2] Joachim Dzubiella,[3] Matthias Schmidt,[4,5] and Alfons van Blaaderen[2]

[1]*Institute of Industrial Science, University of Tokyo, 4-6-1 Komaba, Meguro-ku, Tokyo 153-8505, Japan*
[2]*Soft Condensed Matter, Debye Institute, Utrecht University, Princetonplein 5, 3584 CC, Utrecht, The Netherlands*
[3]*Physics Department (T37), Technical University Munich, James Franck Straße, D-85748 Garching, Germany*
[4]*H.H. Wills Physics Laboratory, University of Bristol, Tyndall Avenue, Bristol BS8 1TL, United Kingdom*
[5]*Institut für Theoretische Physik II, Heinrich-Heine-Universität Düsseldorf, Universitätsstraße 1, D-40225 Düsseldorf, Germany*

We investigate sedimentation of model hard-sphere-like colloidal dispersions confined in horizontal capillaries using laser scanning confocal microscopy, dynamical density functional theory, and Brownian dynamics computer simulations. For homogenized initial states we obtain quantitative agreement of the results from the respective approaches for the time evolution of the one-body density distribution and the osmotic pressure on the walls. We demonstrate that single-particle information can be obtained experimentally in systems that were initialized further out of equilibrium such that complex lateral patterns form.

The process of dispersed particles settling under gravity is a prevalent phenomenon in colloidal dispersions, relevant for isolation of cells from blood [1], separation of macromolecules [2], industrial filtration [3], and the shelf-life of paint [4]. As demonstrated by the beautiful pioneering work of Perrin [5], particles with buoyant mass m that are exposed to a gravitational field with acceleration g can be viewed as being subject to a (linearly) changing local chemical potential $\mu(z) = -mgz + \text{const}$, where z is the height variable. This provides a means to access isotherms and, e.g., study equilibrium phase behavior, provided that the gravitational length, $\xi_g = k_B T/(mg)$, where k_B is the Boltzmann constant, and T is temperature, is large compared to the interparticle correlation length, but small compared to the vertical container size L [6,7]. In equilibrium a pressure gradient that originates from an inhomogeneous density profile, $\rho(z)$, balances gravity and for a dilute dispersion ideal gaslike behavior results, $\rho(z) \propto \exp(-z/\xi_g)$. In concentrated systems, pronounced density oscillations, indicative of liquid layering, occur near the lower wall [8–10].

Understanding the *time evolution* of a given initial state towards sedimentation-diffusion equilibrium is a difficult problem due to the interplay of direct and (solvent-mediated) hydrodynamic interactions between the particles [11]. An isolated sphere of radius a in a solvent of dynamical viscosity η sediments at an average (Stokes) velocity $u_0 = \Gamma_0 mg$, where the mobility is $\Gamma_0 = (6\pi\eta a)^{-1}$ for no-slip boundary conditions on the sphere. Two time scales are of relevance: that of diffusion is the Brownian time it takes a particle to diffuse over a distance of one radius, $\tau_B = 3\pi\eta\sigma^3/(4k_B T)$, and that of gravity is the time it takes a particle to sediment over one radius, $\tau_S = \sigma/(2u_0)$, where $\sigma = 2a$ is the particle diameter. The ratio between both is the Peclet number, $\text{Pe} = \tau_B/\tau_S = a/\xi_g$, that characterizes the type of dynamics. Previous experiments were carried out using sedimenting granular

matter [12] where the effects of diffusion are small (Pe ≫ 1), and using relatively small colloids [11,13] where diffusion dominates (Pe ≪ 1). Steady state in the intermediate regime was recently investigated with computer simulations [14] showing that hydrodynamic backflow effects are relevant but depend little on Pe and that the velocity correlations are similar to those near equilibrium.

In this Letter we investigate full nonequilibrium sedimentation of dispersions inside horizontal planar slits with plate distance L and Pe ∼ 1 using experiment, theory and simulation, all of which are capable of resolving the microscopic structure of the dispersion on the particle level. We obtain quantitative agreement of results from the respective approaches for the strongly inhomogeneous density profiles. This contributes to our understanding of the effects of particle correlations and confinement on the nonequilibrium time evolution of sedimentation and could be relevant for transport of cells in microfluidic devices [15], bacteria in groundwater [16], and in porous media [17].

Our experimental system [18] consists of micronsized, sterically stabilized, fluorescently labeled Poly methyl methacrylate particles [19], dispersed in a mixture of cyclohexyl bromide and *cis*-decalin with 260 μM tetrabutyl ammonium bromide salt to screen the (weak) electrostatic interactions between the colloids, resulting in a Debye screening length of ∼100 nm [18]; see Table I for a summary of all relevant parameters. We tailored the density difference between solvent and particles to control the buoyant mass m and hence Pe. Initially dry capillaries were filled with the suspension; this is a very rapid process due to large capillary forces between the walls and the solvent. The capillaries were laid flat such that the colloids sediment towards the bottom wall, and imaged with a confocal laser scanning microscope; see Fig. 1(a) for an illustration. Confocal scans were made in three dimensions and time series are presented as slices in either vertical [xz, see Fig. 1(b)–1(d)] or horizontal (xy) planes. Coordinates of

TABLE I. Overview of parameters for systems A and B: Total hard sphere packing fraction ϕ_0, scaled density per lateral area $\nu\sigma^2$, where $\phi_0 = \pi\sigma^3\nu/(6L)$, particle diameter σ (in microns) as obtained from static light scattering, capillary spacing L (in microns), scaled gravitational length ξ_g/σ, scaled plate separation distance L/σ, Brownian time τ_B (in seconds), scaled effective (electrostatic) hard sphere diameter $\sigma_{\text{eff}}/\sigma$, and Peclet number Pe. The values for ξ_g/σ, $\sigma_{\text{eff}}/\sigma$, and L/σ are obtained by fitting theoretical results for equilibrium density profiles of hard spheres to those from experiment [33]. The lateral size of the capillaries was 1 mm $\times$ 50 mm.

	ϕ_0	$\nu\sigma^2$	σ	L	ξ_g/σ	L/σ	τ_B (s)	$\sigma_{\text{eff}}/\sigma$	Pe
A	0.15	3.624	3.5	50	0.8	13	57.9	1.05	0.625
B	0.142	10.46	2.8	100	0.45	39.5	29.3	1.1	1.11

the particles were tracked in three dimensions [20], yielding the colloid density profile, $\rho(z, t)$, as a function of the altitude z and time t. We present results for $L/\sigma = 13$ (system A) and $L/\sigma = 39.5$ (system B).

Experimental results for the time evolution of the sedimentation profile for system A are shown in Fig. 2(a). The initial density distribution is almost flat, save for a small peak at the lower wall. This peak grows in time and two more layers appear. The final profile exhibits clear second and third layers and decays smoothly for higher altitudes. We have observed no pronounced changes in the lateral (xy) structure, nor strong fluctuations in particle velocity, in accord with the findings of Ref. [14] and contrasting with the case of strongly driven (steady-state) sedimentation [12].

A recent and very promising theory for the time evolution of the one-body density, $\rho(\mathbf{r}, t)$, where $\mathbf{r}$ is the position coordinate, is dynamical density functional theory [21,22] (DDFT):

$$\frac{\partial\rho}{\partial t} = \nabla \cdot \left(\Gamma\rho\nabla\frac{\delta F[\rho]}{\delta\rho}\right), \tag{1}$$

where Γ is the mobility, $F[\rho]$ is taken to be the equilibrium Helmholtz free energy functional, $F[\rho] = k_B T \int d\mathbf{r}\rho(\mathbf{r}) \times [\ln(\rho(\mathbf{r}, t)\Lambda^3) - 1] + F_{\text{exc}}[\rho] + \int d\mathbf{r}\rho(\mathbf{r})V_{\text{ext}}(\mathbf{r})$, where the first term is the Helmholtz free energy of the ideal gas, Λ is the (irrelevant) thermal wavelength, $F_{\text{exc}}[\rho]$ is the excess (over ideal gas) contribution to the free energy, and the external potential in the present case is $V_{\text{ext}}(\mathbf{r}) = k_B T z/\xi_g$ for $\sigma/2 < z < L - \sigma/2$ and ∞ otherwise. The interparticle interactions are described by the excess free energy functional $F_{\text{exc}}[\rho]$, which we take to be that of hard spheres of diameter $\sigma_{\text{eff}} > \sigma$ to model the (strongly screened) electrostatic repulsion. We use Rosenfeld's successful fundamental-measures theory [23] to approximate $F_{\text{exc}}[\rho]$. As a simple treatment of hydrodynamic interactions we take into account the reduction of Γ upon increasing density with the result by Hayakawa and Ichiki [24], $\Gamma_{\text{HI}}(\phi)/\Gamma_0 = (1 - \phi)^3/[1 + 2\phi + 1.492\phi(1 - \phi)^3]$, where $\phi = 4\pi\rho a^3/3$ is the colloid packing fraction, and we generalize to strongly inhomogeneous situations by using the local packing fraction $\bar{\phi}(\mathbf{r}, t)$, obtained as the convolution of the bare density profile, $\rho(\mathbf{r}, t)$, with a weight function characteristic of the particle volume [23]. We determine values for ξ_g and σ_{eff} such that the theo-

retical result for the equilibrium sedimentation profile [obtained from solving $\delta F[\rho]/\delta\rho(\mathbf{r}) = \mu$ for $\rho(\mathbf{r})$, where μ is the chemical potential] matches its experimental counterpart. The resulting agreement is very good indeed; see the top pair of curves in Fig. 2(a). In addition we have checked that values for σ_{eff} are consistent with our experimental results for the radial distribution function (not shown) and that the values for ξ_g are compatible with those obtained from estimating m from sample composition. We assume $\rho(\mathbf{r}, t) = \rho(z, t)$, take $\rho(z, t = 0)$ to be the equilibrium profile for hard spheres between hard walls without gravity, and integrate Eq. (1) forward in time. The results for $\rho(z, t)$ compare very well with the experimental data, including the time evolution of the layering at the bottom which was not captured in earlier treatments [11], where monotonic density profiles were obtained—as is appropriate on a macroscopic scale.

We further test the DDFT by comparing results for $\rho(z, t)$ to those from Brownian dynamics (BD) simulations. To correct for the finite resolution of the simulations, we have used an intrinsic clock to *measure* time: The clock ticks only when a trial move is accepted, but not when a trial move is rejected due to hard core overlap. We have extensively tested this approach against time step extrapolation [25] and are confident that it is accurate using time steps of $10^{-3}\tau_B$, hence offering significant advantages in computational efficiency. We use a constant mobility $\Gamma_{\text{HI}}(\phi_0)$ both in BD and DDFT, with ϕ_0 being the overall packing fraction. The agreement between results from theory and simulation is remarkable, see Fig. 2(b), establishing for the first time that DDFT is accurate for describ-
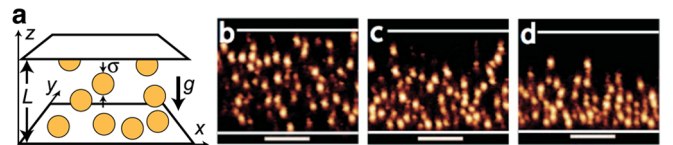

FIG. 1 (color online). Nonequilibrium sedimentation of colloids. (a) Illustration of colloidal spheres of diameter σ under the influence of gravity g and vertically confined between two walls with separation distance L. The vertical coordinate is z; the horizontal coordinates are x and y. (b),(c),(d), Time series of confocal micrographs of system A (see Table I for parameters) taken in the (vertical) xz plane at times $t/\tau_B = 3, 26, 200$, respectively. The scale bars denote 20 μm; the horizontal lines indicate the position of the walls.
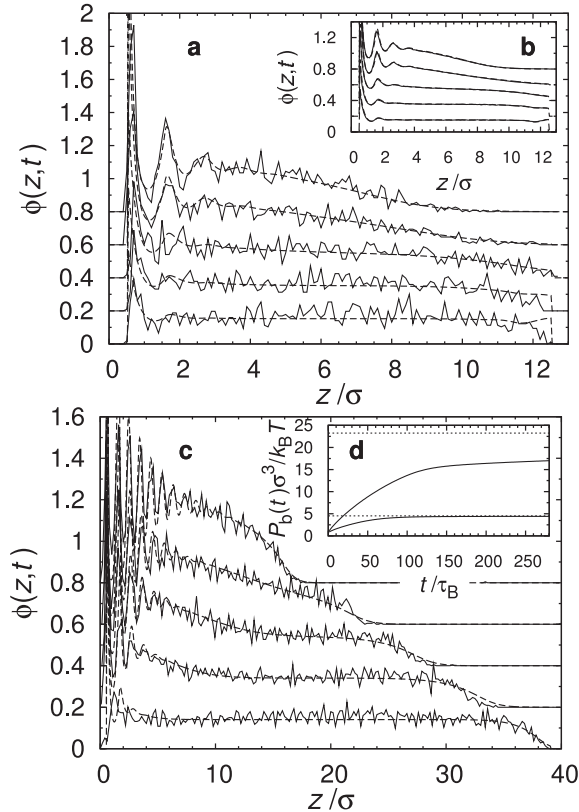
FIG. 2. Time evolution of the density distribution. (a) The local packing fraction $\phi(z, t) = \rho(z, t)\pi\sigma^3/6$ as a function of the (scaled) height coordinate z/σ for (scaled) times $t/\tau_B = 3, 7, 14, 39, 100$ (from bottom to top) for system A. Shown are results from experiment (full lines) and from DDFT using a density-dependent mobility (dashed lines). The curves are vertically offset by 0.2 for clarity. (b) Same as (a) but obtained from BD computer simulations (full lines) and DDFT (dashed lines); in both approaches a constant mobility is used. (c) Same as (a) but for system B for times $t/\tau_B = 7, 26, 44, 63, 255$ (from bottom to top). Time $t = 0$ is set such that the results for the earliest time match; the theoretical curves are scaled with a value of τ_B that is 20% larger than the experimental value. The experimental result for $t = 255\tau_B$ is compared to the theoretical equilibrium profile. (d) The osmotic pressure that the particles exert on the lower wall, $P_b(t)$, as a function of the scaled time, t/τ_B, as obtained from DDFT for system A (lower solid line) and system B (upper solid line). The asymptotic values for $t \to \infty$ are indicated by dotted lines. Results are obtained using a density-dependent mobility.

ing Brownian dynamics of hard spheres in three dimensions; this is both of fundamental and practical importance due to the high computational efficiency of the scheme.

System B serves to investigate the crossover from strongly confined to macroscopic systems. In the early stages we find a large region at intermediate heights where the density remains nearly constant, reminiscent of batch settling [26], as well as a pronounced upper interface of the sediment towards an essentially particle-free supernatant; see Fig. 2(c). For long times pronounced layering at the

bottom of the container develops; we have analyzed the lateral structure in the experiment and have ascertained that these layers remain liquidlike, with no signs of crystallization, which is expected to occur for yet more layers [27]. We achieve very good agreement of the experimental and theoretical results for $\rho(z, t)$, albeit with a small mismatch in time scales: The theoretical results are shown for a value of τ_B that is 20% larger than the experimental value $\tau_B = 29.3$ s, obtained from measurements of particle size and viscosity. The discrepancy might be due to particle size polydispersity ($\sim 5\%$) becoming more important in the case of the larger value of Pe in system B, and not taken into account in the DDFT.

The detailed structural information contained in $\rho(z, t)$ enables us to investigate the time evolution of important macroscopic quantities such as the osmotic pressure [8] exerted by the particles on the bottom and top walls, $P_b(t) = k_B T\rho(z = \sigma/2, t)$ and $P_t(t) = k_B T\rho(z = L - \sigma/2, t)$, respectively. Results shown in Fig. 2(d) indicate a sharp initial increase in $P_b(t)$ with a crossover to slow relaxation for long times towards its equilibrium value, whereas $P_t(t)$ very rapidly decays (not shown). Note that in equilibrium, $P_b - P_t = k_B T\nu/\xi_g$, where ν is the number density per area.

In order to drive the system further out of equilibrium we have altered the initial state by turning equilibrated samples upside down, such that the colloids preferentially reside at the top of the capillary. For this system $\xi_g \approx 0.35\sigma$ and $L \approx 18\sigma$, such that Pe ≈ 1.6. Despite the fact that these parameters are comparable to those considered above, sedimentation proceeds in an entirely different fashion. A strong degree of lateral inhomogeneity develops [28]; see Fig. 3. In the horizontal (xy) plane, see Fig. 3(c), a networklike structure emerges [29]. The structure formation is reminiscent of that resulting from the Rayleigh-Taylor instabililty in two layered liquids, given that the steep initial density gradient resembles that of a liquid-liquid interface. There is likely a relationship between this phenomenon and the swirls observed in sedimenting granular matter [12]. A theoretical investigation of this instability requires an explicit treatment of the lateral x and y coordinates and a more sophisticated handling of the solvent hydrodynamics [30] than only through a density-dependent mobility; these tasks are beyond the scope of the present work. We believe that DDFT, when extended along these lines, could be a very promising candidate for studying such phenomena, both on the grounds of the high accuracy in simpler situations (demonstrated above) and that it also has been used successfully in the past to describe pattern formation in processes such as spinodal decomposition [31].

In conclusion we have presented the first measurements on the single-particle level of sedimentation in model colloidal dispersions. Unlike previous macroscopic descriptions that apply when the gravitational length is much larger than the particle size [11], we have considered
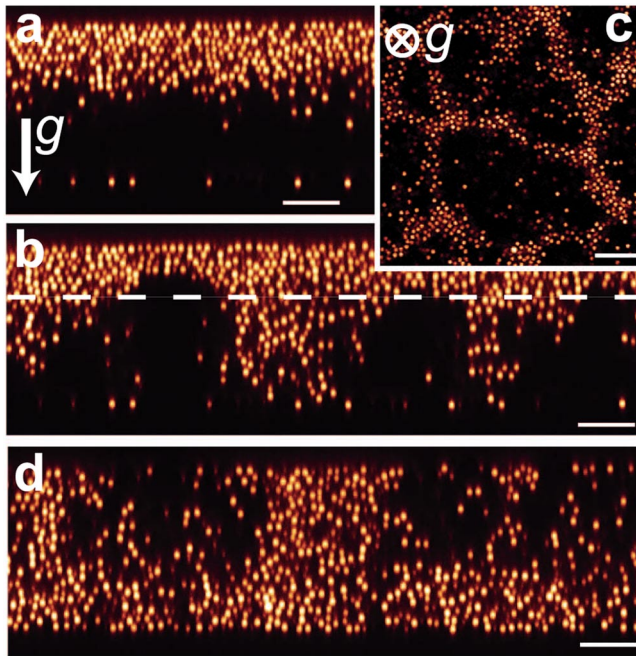
FIG. 3 (color online). Rayleigh-Taylor-like instability. An equilibrated sample is turned upside down and left to sediment [(a) vertical xz plane at time $t = 2\tau_B$]. A strong fingeringlike inhomogeneity develops quickly [(b) vertical xz plane at $t = 5\tau_B$], accompanied by mazelike lateral pattern formation [(c) horizonal xy plane at time $t = 9\tau_B$]. Subsequently, particle diffusion equilibrates the system [(d) vertical xz-plane at time $t = 11\tau_B$], similar to the time evolution shown in Figs. 1(c) and 1(d). The dashed line in (b) indicates the height of the xy plane in (c). The scale bars denote 20 μm; see also [29].

cases where both lengths are similar in magnitude. We have demonstrated that DDFT gives accurate results as compared to computer simulation results and that it describes laterally homogenous sedimentation very well as compared to experimental data. Besides systems that exhibit lateral pattern formation, it would be interesting to investigate in future work larger systems where crystallization occurs as well [27,32].

[1] A. Boyum, Scand. J. Clin. Lab. Invest. **21,** (Suppl. 97), 77 (1968).

[2] Q. G. Wang, H. D. Tolley, D. A. LeFebre, and M. L. Lee, Anal. Bioanal. Chem. **373,** 125 (2002).

[3] F. M. Tiller, N. B. Hsyung, and D. Z. Cong, AIChE J. **41,** 1153 (1995).

[4] P. I. Dolez, A. Goff, and B. J. Love, Sep. Sci. Technol. **37,** 2007 (2002).

[5] J. Perrin, *Atoms* (Constable, London, 1916).

[6] R. Piazza, T. Bellini, and V. Degiorgio, Phys. Rev. Lett. **71,** 4267 (1993).

[7] M. A. Rutgers, J. H. Dunsmuir, J. Z. Xue, W. B. Russel, and P. M. Chaikin, Phys. Rev. B **53,** 5043 (1996).

[8] T. Biben, J.-P. Hansen, and J.-L. Barrat, J. Chem. Phys. **98,** 7330 (1993).

[9] A. Jamnik, J. Chem. Phys. **109,** 11 085 (1998).

[10] N. Choudhury and S. K. Ghosh, J. Chem. Phys. **116,** 384 (2002).

[11] J. K. G. Dhont, *An Introduction to Dynamics of Colloids* (Elsevier, Amsterdam, 1996).

[12] P. N. Segre, F. Liu, P. Umbanhowar, and D. A. Weitz, Nature (London) **409,** 594 (2001).

[13] D. M. E. Thies-Weesie, A. P. Philipse, G. Nägele, B. Mandl, and R. Klein, J. Colloid Interface Sci. **176,** 43 (1995).

[14] J. T. Padding and A. A. Louis, Phys. Rev. Lett. **93,** 220601 (2004).

[15] B. Yao *et al.*, Lab Chip **4,** 603 (2004).

[16] R. W. Harvey *et al.*, Environ. Sci. Tech. **31,** 289 (1997).

[17] J. M. Wan, T. K. Tokunaga, and C. F. Tsang, Water Resour. Res. **31,** 1627 (1995).

[18] C. P. Royall, R. van Roij, and A. van Blaaderen, J. Phys. Condens. Matter **17,** 2315 (2005).

[19] G. Bosma *et al.*, J. Colloid Interface Sci. **245,** 292 (2002).

[20] C. P. Royall, M. E. Leunissen, and A. van Blaaderen, J. Phys. Condens. Matter **15,** S3581 (2003).

[21] U. Marini Bettolo Marconi and P. Tarazona, J. Chem. Phys. **110,** 8032 (1999).

[22] A. J. Archer and M. Rauscher, J. Phys. A **37,** 9325 (2004).

[23] Y. Rosenfeld, Phys. Rev. Lett. **63,** 980 (1989); we obtain the local packing fraction from the volume weighted density $n_3(\mathbf{r})$ as $\tilde{\phi}(\mathbf{r}) = n_3(\mathbf{r})(\sigma/\sigma_{\text{eff}})^3$.

[24] H. Hayakawa and K. Ichiki, Phys. Rev. E **51,** R3815 (1995).

[25] See, e.g., B. Cichocki and K. Hinsen, Physica A (Amsterdam) **166,** 473 (1990).

[26] W. B. Russel, D. A. Saville, and W. R. Schowalter, *Colloidal Dispersions* (Cambridge University Press, Cambridge, England, 1989).

[27] J. P. Hoogenboom, P. Vergeer, and A. van Blaaderen, J. Chem. Phys. **119,** 3371 (2003).

[28] Similar behavior is also observed in computer simulations: H. Tanaka (private communication); A. A. Louis and J. T. Padding (private communication).

[29] See EPAPS Document No. E-PRLTAO-98-051718 for movies exemplifying the dynamics in a vertical and a horizontal plane. For more information on EPAPS, see http://www.aip.org/pubservs/epaps.html.

[30] See, e.g., F. Capuani, I. Pagonabarraga, and D. Frenkel, J. Chem. Phys. **121,** 973 (2004).

[31] A. J. Archer and R. Evans, J. Chem. Phys. **121,** 4246 (2004).

[32] R. P. A. Dullens, D. G. A. L. Aarts, and W. K. Kegel, Phys. Rev. Lett. **97,** 228301 (2006).

[33] The values for L/σ are consistent with those for L within manufacturing tolerances.